Effect of electronic correlations on the spectral and magnetic properties of ZrZn$_2$

S. L. Skornyakov [1,2] V. S. Protsenko [1,2] V. I. Anisimov [1,2] and A. A. Katanin [3,1]

[1]*M. N. Mikheev Institute of Metal Physics of Ural Branch of Russian Academy of Sciences,*
S. Kovalevskaya Street 18, 620990 Yekaterinburg, Russia
[2]*Ural Federal University, 620002 Yekaterinburg, Russia*
[3]*Moscow Institute of Physics and Technology, Institutsky lane 9, Dolgoprudny, 141700 Moscow region, Russia*

We present results of a theoretical study of a prototypical weak ferromagnet ZrZn$_2$. We use the density-functional theory (DFT)+dynamical mean-field theory (DMFT) method to study the electronic and local magnetic properties. The obtained DFT+DMFT electronic self-energies are Fermi-liquid-like, indicating a small effective mass enhancement of the Zr $4d$ states $m^*/m \sim 1.1$–1.3 accompanied by partly formed local moments within the electronic states of t_{2g} symmetry. The effect of electronic interaction is shown to be essential for determining the correct topology of some of the Fermi surface sheets. To study in detail the pressure dependence of the Curie temperature T_C and corresponding pressure-induced quantum phase transition, we consider an effective single-band model, constructed using the Zr $4d$ contribution to the total density of states. The model is studied within static and dynamic mean-field theory, as well as spin-fermion approach. We show that the spin-fermion approach yields the temperature dependence of susceptibility at ambient pressure and the pressure dependence $T_C(p)$, including the first-order quantum phase transition at $p \approx 1.7$ GPa, comparable well with the experimental data.

I. INTRODUCTION

ZrZn$_2$ is a well-known weak ferromagnet. Despite that its magnetic properties have been studied since the 1950s [1], their peculiarities are still actively debated. At ambient pressure this compound is ferromagnetic below the Curie temperature $T_C \approx 30$ K. The ferromagnetism is, however, suppressed by pressure [2] and disappears at $p \approx 1.65$ GPa [3,4]. It was argued in Ref. [5] that the quantum phase transition in ZrZn$_2$ under external pressure is in fact of the first order; at finite magnetic field the corresponding metamagnetic behavior is observed [5,6]. Near the quantum phase transition in zero magnetic field the exponent of the resistivity $\rho \propto T^\alpha$ changes [4] from the value $\alpha = 5/3$, which is characteristic for systems with ferromagnetic correlations [7,8], to $\alpha = 3/2$, characteristic for antiferromagnetic correlations.

Density-functional theory (DFT) band structure calculations [9,10] of ZrZn$_2$ revealed an extended van Hove singularity due to a flat part of dispersion near the L point of the Brillouin zone, similar to that in nickel [11]. This flat part yields a peak of the density of states near the Fermi level [10,12], characteristic to many ferromagnetic materials. This peak on one hand promotes ferromagnetism [13], but on the other hand, it makes the Stoner theory even qualitatively inapplicable at finite temperatures, since competing channels of electron scattering become important in this situation, as it was studied actively in two-dimensional systems with van Hove singularities [14]. In general, Stoner theory predicts transition temperatures much larger than the corresponding experimental data and does not explain the linear temperature dependence of inverse susceptibility [8], which points to the

importance of correlation effects. The lowest-order paramagnon interaction was described within the Moriya theory [8]. This theory was justified within the renormalization group method [15] and allowed to predict the universal behavior of weak itinerant magnets near quantum phase transitions. At the same time, for numerical predictions of nonuniversal properties it requires the knowledge of both the electronic dispersion and the (para)magnon spectrum. Moriya theory was also extended to include the effect of higher-order diagrams with respect to paramagnon interaction (expressed through the density of states for sufficiently large correlation lengths) [16–19].

However, these spin-fluctuation approaches were not intensively applied to models with realistic densities of states; they also may be insufficient by the following reasons: (i) above mentioned interplay of different channels of electron scattering can yield a strong renormalization of particle-hole spin excitations by other channels of electron interaction; (ii) strong on-site correlations are not considered by these approaches. In particular, in the multiorbital case the correlation-induced physics is more reach due to the Hund interaction which may trigger for example the Hund metal behavior [20–22], characterized by (orbital-selective) formation of local moments. Although in weak magnets the effect of Hund exchange is expected to be less dramatic than in strong magnetic materials, it should also be considered.

Therefore, weak ferromagnets pose a challenge for theoretical studies since both local and nonlocal correlations are expected to be essential to describe their properties. Accordingly, at least two aspects of weak itinerant magnetism should be investigated. The first aspect is the role of strong

local Coulomb interaction and peculiarities of realistic density of states for quasiparticle and magnetic properties. For that, state-of-the-art methods for calculation of electronic properties based on a combination of density functional theory and dynamical mean-field theory of correlated electrons (DFT+DMFT) [23–25] have shown to be a powerful theoretical tool for studying the physics of real materials [26]. The second aspect is the applicability of effective single-band models with realistic densities of states and a possibility to use them to study magnetic properties of weak itinerant magnets.

In this paper, we explore the effect of local Coulomb correlations on the electronic and magnetic properties of $ZrZn_2$ (space group $Fd\bar{3}m$) within the DFT+DMFT method. We interpret the results of multiorbital DFT+DMFT calculation within the effective one-band model constructed using the realistic density of states of $ZrZn_2$ and solved by DMFT. To understand details of the paramagnet to ferromagnet transition we furthermore study an effective one-band model within static mean field and spin-fermion model approaches.

The paper is organized as follows. In Sec. II A we describe the technical details of our DFT+DMFT calculations. The corresponding results for spectral properties, local and nonuniform spin susceptibility, and temperature dependence of the uniform spin susceptibility of $ZrZn_2$ are discussed in Sec. II B. The effective single-band model is considered in Sec. III within DMFT (Sec. III A), mean-field approach (Sec. III B), and spin-fermion model (Sec. III C). Finally, our results are summarized in Sec. IV. In Appendix A we discuss behavior of the uniform particle-hole bubble at not too low temperatures, while in Appendix B we provide details on the equations of the spin-fermion model used to account for the effect of spin fluctuations.

II. DFT+DMFT STUDY

A. Method

We first study the effect of local electronic correlations on the electronic structure and magnetic properties of $ZrZn_2$. For that we have employed the DFT+DMFT method implemented within the plane-wave pseudopotential approach with generalized gradient approximation (GGA) in DFT [27]. We used a basis set of Wannier functions constructed by means of the projection procedure [28,29] for an energy window spanning occupied Zn $3d$ and partially filled Zr $4d$ bands. The realistic DFT+DMFT many-body problem is solved by the continuous-time hybridization-expansion quantum Monte-Carlo method (CT-QMC, segment algorithm) [30]. In these calculations we neglect effects of spin-orbit coupling. The Coulomb interaction term has been treated in the density-density approximation with the average Hubbard interaction $U = 2.5$ eV and Hund's exchange $J = 0.3$ eV for the Zr $4d$ orbitals [31]. To account for Coulomb interaction energy already described by DFT we employ the fully-localized double-counting correction $V_{dc} = U(N_d - 0.5) - 0.5J(N_d - 1)$ self-consistently evaluated from local occupations N_d. We have verified that using the around-mean-field form of the double counting term does not change essentially our results. Spectral functions and orbital-dependent band mass renormalizations were computed using the real-axis
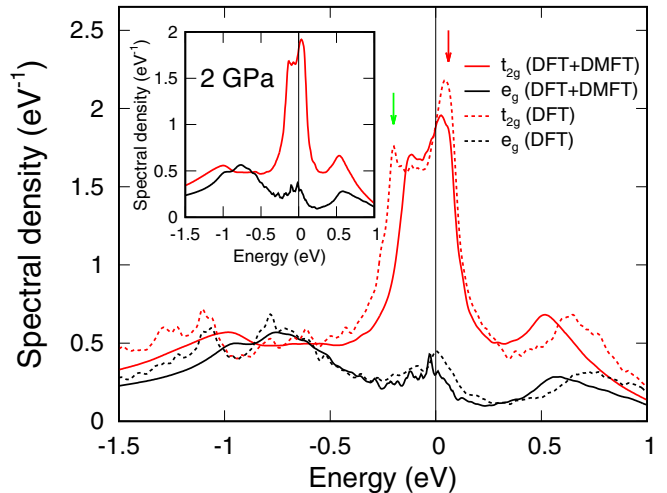

FIG. 1. Comparison of orbitally-resolved spectral functions of paramagnetic $ZrZn_2$ computed by DFT+DMFT ($T = 464$ K) and DFT at ambient pressure. The inset shows DFT+DMFT results obtained at $p = 2$ GPa. The Fermi energy is set to 0 eV.

self-energy $\hat{\Sigma}(\nu)$ obtained from the Padé analytical approximation of the DFT+DMFT imaginary-axis self-energy $\hat{\Sigma}(i\nu)$ [32]. In order to determine the lattice parameter of cubic $ZrZn_2$ under pressure we compute the total energy as a function of volume using the GGA energy functional and shift the experimental lattice constant according to the third-order Birch-Murnaghan equation of state [33]. For simplicity, only hydrostatic contraction and expansion of the cubic unit cell are considered in these calculations.

Within DFT+DMFT we compute the uniform magnetic susceptibility as a derivative of the field-induced magnetization $M(T)$ with respect to the applied field H:

$$\chi(T) = \frac{\partial M(T)}{\partial H} = \mu_B^2 \frac{\partial[n_\uparrow(T) - n_\downarrow(T)]}{\partial E_h}, \qquad (1)$$

where $n_\sigma(T)$ is the occupation of the spin-σ at a temperature T, $E_h = \mu_B H$ is the bare splitting of electronic spectrum, and μ_B is the Bohr magneton. In these calculations we check an absence of polarization in the zero field and the linear character of M as a function of E_h.

B. Results

1. Electronic properties

As a starting point, we discuss the effect of electronic correlations on the electronic properties of $ZrZn_2$. The spectral functions of $ZrZn_2$ calculated by DFT and DFT+DMFT for the experimental crystal structure are presented in Fig. 1. In agreement with previous theoretical investigations [12,34] our results (both DFT and DFT+DMFT) show that the spectral weight in the vicinity of the Fermi energy (E_F) is due to the Zr $4d$ orbitals and mostly originates from the t_{2g} states. These orbitals form a narrow band located in the interval $(-0.5, 0.5)$ eV with sharp peaks below and above the E_F (marked by arrows in Fig. 1). The e_g spectral function also shows a broad peaked feature above the Fermi level, but its amplitude is almost five times smaller than that due to the t_{2g}
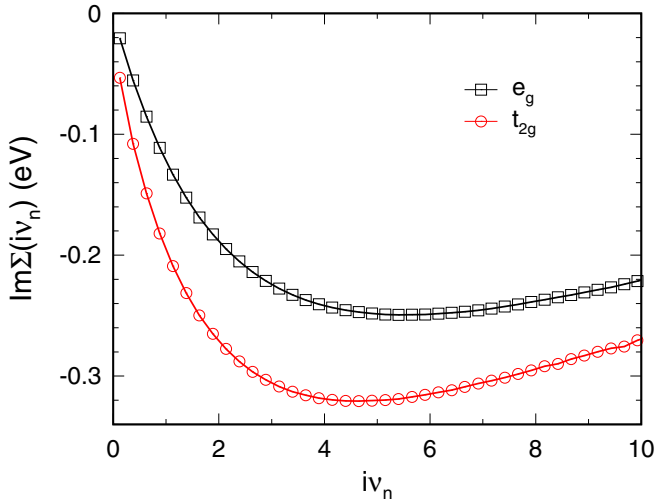
FIG. 2. Orbitally-resolved imaginary parts of the local self-energy of paramagnetic $ZrZn_2$ at ambient pressure on the Matsubara mesh obtained with DFT+DMFT ($T = 464$ K).

states. In addition, we observe that the Zn-$3d$ band is located well below E_F and is weakly hybridized with Zr-$4d$ states close to the Fermi level.

The Zr-$4d$ spectral functions computed by DFT+DMFT share a common shape with those obtained within DFT. Correlation effects only lead to a shift and renormalization of the quasiparticle bands near E_F and do not induce a significant transfer of the spectral weight. In particular, we observe that the sharp peak originating from the t_{2g} states emerges at ~ 0.025 eV, almost twice closer to E_F compared to its position in DFT (~ 0.05 eV). Such an effect of shifting the peak of the density of states towards the Fermi level is common for other correlated metallic systems. For example, it occurs in α- [35], γ- [36], ϵ-iron [37], FeAl [38], and some two-dimensional systems (see, e.g., Refs. [39–41]). The e_g spectral function shows a similar transformation. However, the e_g-derived peak is pushed from above to below the Fermi energy. The obtained shape of the spectral functions is preserved in the whole pressure range $p < 2$ GPa with all the features shifted to higher energies with increasing pressure. In particular, at $p = 2$ GPa the peak of the e_g states reaches the Fermi level.

To quantify electronic correlations in $ZrZn_2$ we analyze the local DFT+DMFT self-energy $\hat{\Sigma}(i\nu_n)$ and the effective band mass enhancement $m^*/m = 1 - \partial \text{Im} \hat{\Sigma}(i\nu)/\partial(i\nu)|_{i\nu \to 0}$. Here $i\nu_n$ is the fermionic Matsubara frequency and the derivative $\partial \text{Im} \hat{\Sigma}(i\nu)/\partial(i\nu)$ is computed using Padé extrapolation of $\hat{\Sigma}(i\nu)$ to $i\nu = 0$. Our results for the frequency dependence of orbitally-resolved self-energies $\text{Im}\hat{\Sigma}_m(i\nu_n)$ ($m = t_{2g}, e_g$) at an electronic temperature $T = 464$ K are presented in Fig. 2. We observe that the e_g self-energy exhibits a Fermi-liquid-like behavior with insignificant damping of quasiparticles ($\text{Im}\hat{\Sigma}_{e_g}(0) \sim 0.002$ eV) and yields the mass enhancement $m^*/m = 1.16$. The t_{2g} states are less coherent and show a stronger renormalization with $\text{Im}\hat{\Sigma}_{t_{2g}}(0) \sim 0.015$ eV and $m^*/m = 1.34$.

We proceed further with investigation of the effect of electronic correlations on the Fermi surface (FS) and band structure of $ZrZn_2$. To compute the FS within DFT+DMFT
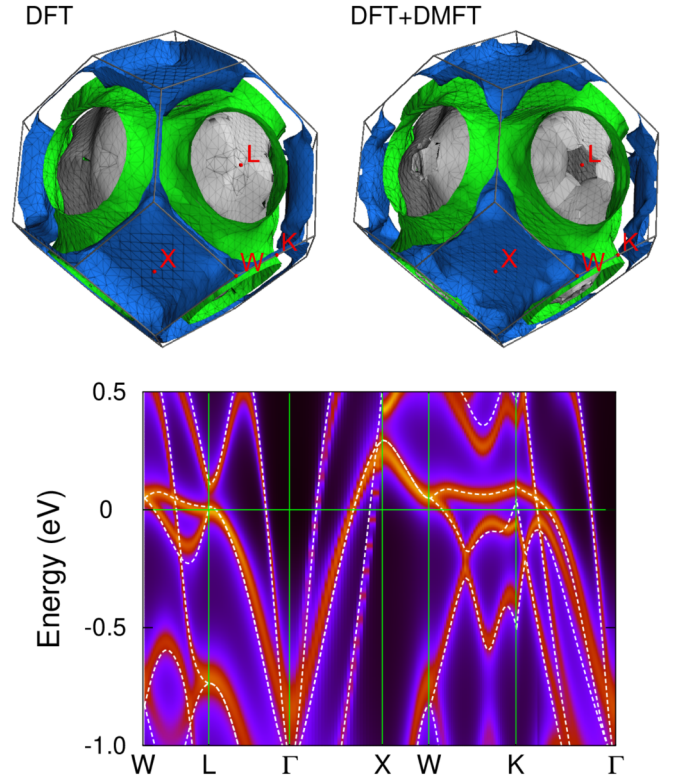

FIG. 3. Upper panel: Fermi surface of $ZrZn_2$ at ambient pressure as obtained within DFT (left) and that computed by DFT+DMFT at $T = 464$ K (right). Lower panel: Band structure of paramagnetic $ZrZn_2$ computed by DFT+DMFT at $T = 464$ K (contours) and DFT (dashed lines).

we locate poles of the analytically continued lattice Green function $G_{\mathbf{k}}(\nu = 0)$, diagonalized in the orbital space. In Fig. 3 (upper panel) we compare our results for the FS calculated by DFT and DFT+DMFT at ambient pressure. Both DFT and DFT+DMFT approaches yield the FS that shows four sheets centered at the Γ point. Specifically, the FS consists of the innermost spherical sheet (not seen in Fig. 3) surrounded by three other sheets with more complex shape. We observe that upon inclusion of electronic correlations topology of the inner sheet (Fig. 3, gray) changes near the L point and the outer sheet (Fig. 3, blue) splits along the $W - K$ direction of the Brillouin zone, such that the DFT+DMFT Fermi surfaces are in agreement with experimental data [42]. Analysis of the band structure (Fig. 3, lower panel) shows that this transformation occurs due to a correlation-induced shift of the bands at the L and K points of the Brillouin zone, from above to below the Fermi level. Therefore, correlations are crucially important to obtain the correct topology of the Fermi surface of $ZrZn_2$ (see also discussion in Ref. [42]).

2. Local spin susceptibility

We consider further the local spin susceptibility $\chi(\tau) = \langle \hat{s}_i^z(\tau) \hat{s}_i^z(0) \rangle$ [where $\hat{s}_i^z(\tau)$ is the instantaneous spin at the site i at imaginary time τ and $\langle \ldots \rangle$ denotes the thermal average computed by CT-QMC] and its Fourier transform $\chi_{\text{loc}}(i\omega_n) = \int_0^{1/k_B T} \chi(\tau) \exp(i\omega_n \tau) d\tau$, ω_n being bosonic Matsubara frequencies. Our results for the temperature dependence of the
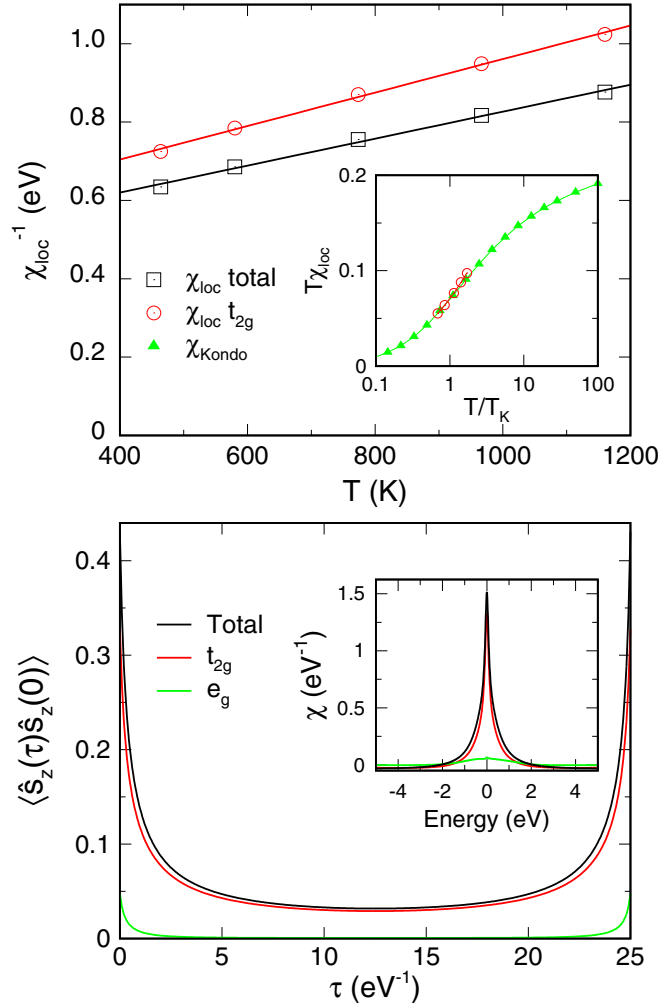
FIG. 5. Momentum dependence of the particle-hole bubble $\chi_{\mathbf{q}}^0$ in ZrZn$_2$ computed by DFT+DMFT at ambient pressure (a.p.) and 2 GPa.

FIG. 4. Upper panel: Temperature dependence of the inverse local spin susceptibility χ_{loc}^{-1} of paramagnetic ZrZn$_2$ and the inverse of the corresponding t_{2g} contribution, computed by DFT+DMFT. The inset shows a fit of the t_{2g} contribution to local susceptibility (circles) by the universal dependence $T\chi_{\mathrm{loc}}(T/T_{\mathrm{K}})$ for the Kondo model [43] (triangles), allowing us to obtain the Kondo temperature T_{K}. Lower panel: Local spin correlation function $\chi(\tau) = \langle \hat{s}_i^z(\tau)\hat{s}_i^z(0)\rangle$ of paramagnetic ZrZn$_2$ as computed by DFT+DMFT at $T = 464$ K. Orbitally-resolved Fourier transform of $\chi(\tau)$ as a function of the real energy is shown in the inset.

the analytical continuation of $\chi(\omega)$ at the half height [36] and it is equal to 0.16 eV. This value corresponds to the lifetime 25 fs, which is approximately twice longer than that discussed previously for the iron pnictides [44] and ϵ-iron [37] but much shorter than the lifetime of local moments in such strong magnet as α-iron [35]. At the same time, almost no local moments are formed in the e_g states. These results are in line with orbital-selective behavior of the self-energy and imply a different degree of electronic coherence for different orbitals of the Zr 4d shell, indicative for orbital-selective local moments.

3. Momentum dependence of the nonuniform magnetic susceptibility

To study preferable types of magnetic correlations in ZrZn$_2$, in Fig. 5 we show the momentum dependence of the nonuniform magnetic susceptibility, represented by the particle-hole bubble,

$$\chi_{\mathbf{q}}^0 = -\left(2\mu_{\mathrm{B}}^2/\beta\right)\sum_{\mathbf{k},\nu_n}\mathrm{Tr}[\hat{G}_{\mathbf{k}}(i\nu_n)\hat{G}_{\mathbf{k+q}}(i\nu_n)], \qquad (2)$$

where $\hat{G}_{\mathbf{k}}(i\nu_n)$ is the one-particle DFT+DMFT Green function on Zr atom, which is a matrix in the space of d orbitals, $\beta = 1/k_{\mathrm{B}}T$. One can see that apart from the peak at $\mathbf{q}_\Gamma = 0$, which shows a tendency to ferromagnetic order, there is a strong peak of $\chi_{\mathbf{q}}^0$ at $\mathbf{q}_L = (\pi, \pi, \pi)$, showing the presence of spin density wave correlations. Detail analysis of contribution of different momenta shows that this peak originates from the nesting between wide necks of the FS sheets close to the $W - K$ edge of the Brillouin zone (Fig. 3, green) and corners of the pillowlike FS centered at the X points (Fig. 3, blue). The tendency towards spin density wave may explain the experimentally observed $T^{3/2}$ dependence of the resistivity in the paramagnetic state under pressure [4].

4. Uniform magnetic susceptibility

To complement the analysis of magnetic properties of ZrZn$_2$ we consider the temperature dependence of inverse uniform magnetic susceptibility $\chi^{-1}(T)$. In Fig. 6 we compare

inverse static local spin susceptibility $\chi_{\mathrm{loc}}^{-1} = (\chi_{\mathrm{loc}}(0))^{-1}$ are shown in Fig. 4 (upper panel). Calculated χ_{loc}^{-1} and the corresponding inverse partial contributions of t_{2g} and e_g states to a good approximation are linear functions of temperature. The contribution of e_g states to the susceptibility (not shown) is much smaller than that of the t_{2g} states. From the fit of the t_{2g} contribution by the universal temperature dependence $T\chi_{\mathrm{loc}}(T/T_{\mathrm{K}})$ of the impurity susceptibility of the Kondo model [43], we find a rather large Kondo temperature $T_{\mathrm{K}} \approx 680$ K, which shows that local moments are fully screened at low temperatures. The presence of a flat part of time dependence of $\chi(\tau)$ (see lower panel of Fig. 4) is indicative of short-lived local moments in the t_{2g} band. Their inverse lifetime is characterized by the half width of the peak of
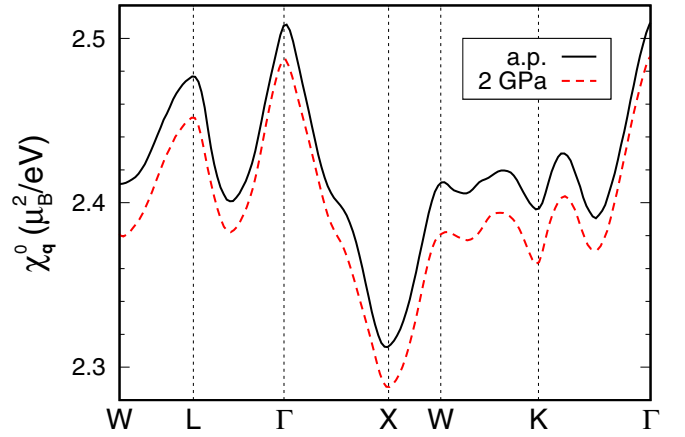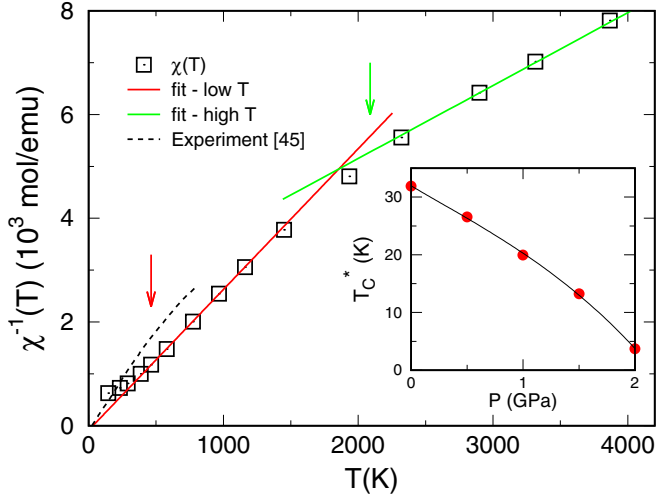
FIG. 6. Temperature dependence of the inverse uniform spin susceptibility $\chi^{-1}(T)$ of paramagnetic $ZrZn_2$ computed by DFT+DMFT at ambient pressure (squares) in comparison with experiment (broken line) [45]. The straight solid lines represent least-square fits to $\chi^{-1}(T)$ in the temperature range [400,1200] K and [2000,4000] K. Temperatures corresponding to excitation energies of the peaks in the density of states are indicated by arrows. The inset shows the pressure dependence of T_C^* as calculated from the low-temperature fit of $\chi^{-1}(T)$.

our DFT+DMFT results for $\chi^{-1}(T)$ to experimental data of Shimizu *et al.* [45]. To highlight the regions of Curie-Weiss behavior, we show least square linear fits to the computed points. One can see that the Curie-Weiss law is fulfilled at $T > T_{CW} \approx 400$ K; the slope of inverse susceptibility changes at the temperature $T'_{CW} \approx 2000$ K. The temperatures T_{CW} and T'_{CW} approximately correspond to the energy of the two peaks of the DFT t_{2g} density of states, closest to the Fermi level ($\varepsilon_1 \approx -0.15$ eV and $\varepsilon_2 \approx 0.05$ eV, respectively), cf. Fig. 1. The reason for the change of magnetic susceptibility at $T = T_{CW}$ and T'_{CW} is that the electronic correlations are strongly enhanced by peaks of the density of states.

At $T > T'_{CW}$ we find a magnetic moment $\mu = 2.38\,\mu_B$. This value corresponds to weakly interacting electrons [$\mu = 2.39\,\mu_B$ is obtained from the lowest order bubble contribution (2) for Zr states, relevant in the considered temperature range, see Appendix A]. At the same time, at $T_{CW} < T < T'_{CW}$ we find a reduced magnetic moment $\mu = 1.72\,\mu_B$. Via the relation

$$\mu^2 = (g\mu_B)^2 p(p+1), \tag{3}$$

where $g = 2$, this value corresponds to an effective spin $p = 0.49$. This value can be interpreted as corresponding to a correlated electronic state with partial localization of one hole in the t_{2g} band (filling $n_{t_{2g}} = 4.5$), which agrees with the discussion in Sec. II B 2.

The slope of $\chi^{-1}(T)$ in the range $T_{CW} < T < T'_{CW}$, and, therefore, the respective magnetic moment, is in agreement with experimental data, although with some shift of the inverse susceptibility, which origin is to be clarified by future investigations. Orbitally resolved contributions χ_α ($\alpha = t_{2g}$, e_g) to the total susceptibility (not shown) indicate that the temperature evolution of $\chi(T)$ in a wide temperature range mostly originates from the t_{2g} orbitals. The contribution of the e_g states is an order of magnitude smaller and becomes notable only in the low-temperature region.

At lower temperatures $T < T_{CW} \sim T_K$ theoretical $\chi^{-1}(T)$ dependence shows an upturn, which is likely related to the Kondo screening of the local moment formed by t_{2g} states. Such upturn is found in DFT+DMFT studies of many Hund metals with van Hove singularity, slightly shifted off the Fermi level [36–38,40,46], although it is not observed in the experimental temperature dependence of the susceptibility of $ZrZn_2$. The obtained upturn of $\chi^{-1}(T)$ at low temperatures physically implies a tendency towards a nonferromagnetic ground state. Our results demonstrate that this tendency, which originates from the Kondo screening of local moment, formed by the t_{2g} states, is overestimated in the DMFT approach for $ZrZn_2$. As a result, DFT+DMFT is applicable to the considered system only at not too low temperatures.

To proceed further with the results of DFT+DMFT approach, we extract a characteristic temperature T_C^* of the onset of strong ferromagnetic correlations (which is approximately identified with the Curie temperature T_C) by extrapolating the dependence of susceptibility at high temperatures according to the Curie-Weiss law, $\chi^{-1} \propto T - T_C^*$. The extrapolation of the fit to $\chi^{-1} = 0$ at ambient pressure gives the temperature $T_C^* \sim 32$ K, close to the value reported in Ref. [45].

Upon increasing pressure we observe a growth of $\chi^{-1}(T)$ in the temperature range $T < 1200$ K. The effect of pressure is accompanied by a monotonic reduction of T_C^* (Fig. 6, inset). In particular, at $p = 1$ GPa we obtain a drop of T_C^* to ~20 K which further develops to ~4 K at $p = 2$ GPa. This behavior is in overall qualitative agreement with experimental tendency of decreasing the Curie temperature under compression of the lattice [3–6].

Reconciling the results of DFT+DMFT approach with the experimental data at low temperatures requires consideration of nonlocal correlations. The treatment of nonlocal spin correlations within the spin-fermion model is presented below, in Sec. III C. In Sec. IV we also discuss possible reasons of inapplicability of DMFT in the low-temperature region.

III. EFFECTIVE SINGLE-BAND MODEL

A. The model and the dynamical mean-field theory

To study the phase transition to ferromagnetic phase in more detail, we consider an effective single-band model. To construct this model we use a cut of the realistic total density of states of $ZrZn_2$ computed by DFT in an energy window chosen to span the full width of Zr-4d band. The normalized density of states $\rho(\epsilon)$ (Fig. 7, upper panel) defines a single-band model which is solved by dynamical and static mean-field theory, as well as investigated within the spin-fermion model approach. In these calculations the occupation at each pressure is fixed at its value obtained by using the Fermi level position in DFT calculation (e.g., at $p = 0$ GPa after normalization this procedure yields a total occupation $n = 1.56$, which is close to the averaged occupation of Zr-d Wannier states).
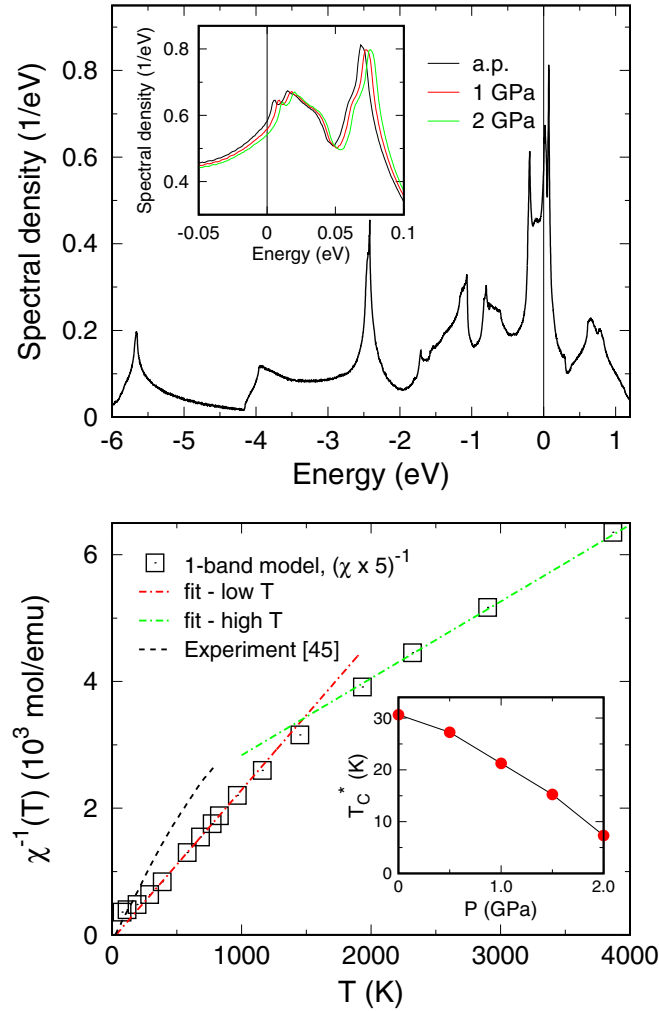
FIG. 7. Top: Noninteracting density of states of a one-band model at ambient pressure (a.p.) and its evolution close to the Fermi level (0 eV) at $p = 1$ GPa and $p = 2$ GPa (inset). Bottom: Temperature dependence of the inverse uniform susceptibility $\chi^{-1}(T)$ of the one-band model as computed by DMFT at ambient pressure using the Coulomb parameter $U = 4.5$ eV (squares). The dot-dashed lines show linear fits; the dashed line corresponds to the experimental data of Ref. [45]. The inset shows the pressure dependence of T_C^* extracted from a linear fit to the low-temperature part of $\chi^{-1}(T)$.

In the dynamical mean-field theory we consider a standard single-impurity Anderson model (AIM), supplemented by the self-consistency condition $\int \rho(\epsilon)/(i\nu_n - \epsilon - \Sigma(i\nu_n)) = g(i\nu_n)$ where $g(i\nu_n)$ is the local Green's function and $\Sigma(i\nu_n)$ is the local self-energy, obtained within the AIM. We note that previously a similar approach was used for study a ferromagnetic instability in systems with model densities of states [47]. Here, we use the *ab initio* density of states $\rho(\epsilon)$, constructed as discussed above. To compare our DMFT results for the single-band model with those of Sec. II B for a realistic multiband model, we use in the DMFT approach to the single band model the local Coulomb interaction $U = 4.5$ eV chosen such that the value of characteristic temperature T_C^* at ambient pressure is close to that obtained for the multiband model.

The corresponding DMFT results for the inverse spin susceptibility, multiplied by a number of relevant orbitals of the

real compound, i.e., $[5\chi(T)]^{-1}$, are shown in Fig. 7, lower panel. These results are quite similar to those of the multiorbital model. In particular, in the low-temperature region the computed inverse susceptibility shows an upturn in the low-temperature region. We note that similar upturn was obtained also in earlier studies of the single-band Hubbard model with the peak of the density of states shifted off the Fermi level [40]. By analogy to the multiorbital case we extract the characteristic temperature T_C^* of the onset of strong ferromagnetic correlations from a linear fit of the low-temperature part of $\chi^{-1}(T)$. At ambient pressure our calculations yield $T_C^* \sim 30$ K which drops to ~ 7 K at $p = 2$ GPa in qualitative agreement with the realistic DFT+DMFT calculation (Fig. 7, lower panel, inset). Studying the paramagnetic to ferromagnetic phase transition requires an account for nonlocal correlations supplemented by a comparison of energies of para- and ferromagnetic states. We note that the importance of nonlocal correlations for stability of ferromagnetism was emphasized earlier in the DMFT study of a single-band model in Ref. [47]. As we show in the following subsections the transition to the ferromagnetic state can be successfully described by employing a simplified spin-fermion model.

B. Mean-field approximation

Before analyzing magnetic properties of the single-band model within the spin-fermion approach, we consider the static mean-field approximation, described by the action

$$\mathcal{S}_{\mathrm{MF}} = \sum_{k,\sigma} c_{k,\sigma}^{\dagger}(-i\nu_n + \epsilon_{\mathbf{k}} - \mu)c_{k,\sigma} + U(n_{\uparrow}n_{\downarrow})_{\mathrm{MF}}, \quad (4)$$

where $c_{k,\sigma}^{\dagger}, c_{k,\sigma}$ are Grassmann variables, ν_n are fermionic Matsubara frequencies,

$$(n_{\uparrow}n_{\downarrow})_{\mathrm{MF}} = \langle n_{\uparrow}\rangle n_{\downarrow} + \langle n_{\downarrow}\rangle n_{\uparrow} - \langle n_{\uparrow}\rangle\langle n_{\downarrow}\rangle$$
$$= n\langle n\rangle/2 - 2\langle s_z\rangle s_z - \langle n\rangle^2/4 + \langle s_z\rangle^2, \quad (5)$$

$n = n_{\uparrow} + n_{\downarrow}$, $\quad s_z = (n_{\uparrow} - n_{\downarrow})/2$, $\quad n_{\sigma} = \sum_k c_{k,\sigma}^{\dagger}c_{k,\sigma}$, $k = (\mathbf{k}, \nu_n)$ is the momentum-frequency 4-vector, $\epsilon_{\mathbf{k}}$ is an electronic dispersion of the one-band model, and μ is the chemical potential. This leads to well-known self-consistent equations for $\langle n\rangle$ and $\langle s_z\rangle$,

$$\langle n\rangle = \sum_{\sigma} \int f(\tilde{\epsilon} + \sigma U\langle s_z\rangle)\rho(\epsilon)d\epsilon, \quad (6a)$$

$$\langle s_z\rangle = -\frac{1}{2}\sum_{\sigma} \sigma \int f(\tilde{\epsilon} + \sigma U\langle s_z\rangle)\rho(\epsilon)d\epsilon, \quad (6b)$$

where $\quad \tilde{\epsilon} = \epsilon - \mu + U\langle n\rangle/2$, $\quad \sigma = \pm 1$, $\quad f(\epsilon) = (1 + \exp(\beta\epsilon))^{-1}$ is the Fermi function, and $\rho(\epsilon)$ is the density of states per one spin projection.

We solve the equations (6) for μ and $\langle s_z\rangle$ for a given electron concentration per orbital $\langle n\rangle$, obtained in DFT calculations. This yields paramagnetic (μ_{PM}, $\langle s_z\rangle = 0$) and ferromagnetic (μ_{FM}, $m_{\mathrm{FM}} = \langle s_z\rangle \neq 0$) solutions. To find an energetically preferable solution, we compare the values of
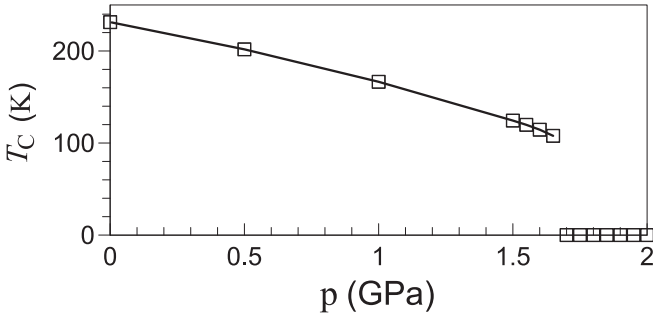
FIG. 8. Pressure dependence of the Curie temperature $T_C(p)$ in the mean-field analysis of the single-band model for $U = 1.8$ eV.

thermodynamic potential

$$\Omega(\mu; \langle n \rangle, \langle s_z \rangle) = U(\langle s_z \rangle^2 - \langle n \rangle^2/4)$$

$$- \beta^{-1} \sum_\sigma \int \ln[1 + e^{-\beta(\tilde{\epsilon} + \sigma U \langle s_z \rangle)}]\rho(\epsilon)d\epsilon. \quad (7)$$

If $\Omega(\mu_{PM}; \langle n \rangle, 0) < \Omega(\mu_{PM}; n_{PM}, \langle s_z \rangle_{PM})$, where n_{PM} and $\langle s_z \rangle_{PM} \neq 0$ fulfill the mean-field equations for $\mu = \mu_{PM}$, then the paramagnetic solution is considered energetically preferable, while in case $\Omega(\mu_{FM}; \langle n \rangle, m_{FM}) < \Omega(\mu_{FM}; n_{FM}, 0)$, where n_{FM} and $\langle s_z \rangle = 0$ is the solution of MF equations for $\mu = \mu_{FM}$, the ferromagnetic solution dominates.

Solution of the equations (6) and (7) in the ground state for moderate Coulomb interaction shows that the ferromagnetic ground state is energetically preferable for positions of the peak of the density of states close to the Fermi level (sufficiently low pressures), while paramagnetic state is energetically preferable for peak positions far from the Fermi level.

We note that the effective interaction U in the static mean-field theory is typically smaller than the bare Coulomb interaction of the one-band model, since it accounts for the screening processes, cf. Refs. [48,49]. We choose below the effective Coulomb interaction $U = 1.8$ eV from the condition that the first-order quantum phase transition occurs at the pressure p_c close to the experimental value $p_c = 1.65$ GPa.

The calculated dependence of Curie temperature $T_C(p)$ in the mean-field theory is presented in Fig. 8. The obtained pressure dependence of T_C is in qualitative agreement with the experimental data [5,6]. However, the obtained Curie temperatures overestimate experimental values by an order of magnitude, which is usual for mean-field theory of weak magnetic systems [8]. In the narrow region of pressures near quantum phase transition, where none of the above criteria of preference of paramagnetic or ferromagnetic solution is fulfilled, the phase separation between para- and ferromagnetic phases occurs. We do not study this region in details since it is rather narrow for ZrZn$_2$.

C. Spin-fermion model

To improve the results of the mean-field approximation, let us take into account the effect of spin fluctuations in the spin-fermion model. To this end, we consider the partition function

$$Z = \int \mathcal{D}[c, c^\dagger] \int d^3\tilde{S} \exp(-\beta \mathcal{S}_{eff}) \quad (8)$$

with the effective action

$$\mathcal{S}_{eff} = \mathcal{S}_{MF} + 2U\mathbf{s}\tilde{\mathbf{S}} + D\tilde{\mathbf{S}}^2, \quad (9)$$

containing the fluctuating field $\tilde{\mathbf{S}}$; $\mathbf{s} = (1/2)\sum_{k,\sigma,\sigma'} c^\dagger_{k,\sigma} \boldsymbol{\sigma}_{\sigma\sigma'} c_{k,\sigma'}$ corresponds to the spin of itinerant degrees of freedom, $\boldsymbol{\sigma} = (\sigma_x, \sigma_y, \sigma_z)$ is the vector of Pauli matrices, and D is the strength of spin fluctuations. For simplicity we consider here only the effect of spin fluctuations of static uniform ($\mathbf{q} = 0$, $\omega_n = 0$) spin mode, which can be justified at sufficiently large correlation lengths [16–19,50]. We also note that at finite temperatures the classical fluctuations in dimension $d = 3$ are relevant from the renormalization group point of view, in contrast to quantum fluctuations, having dimension $d + z$, where $z = 3$ is the dynamic critical exponent [15]. To be consistent with the mean-field action (4), we keep the spin-fermion interaction equal to $2U$, cf. Ref. [18]. This yields the following equations for the electronic density and the magnetization in the absence of magnetic field (see Appendix B)

$$\langle n \rangle = A \int d^3\tilde{S} \exp(-\beta D\tilde{\mathbf{S}}^2)$$

$$\times \sum_\sigma \int f(\tilde{\epsilon} + \sigma\gamma)\rho(\epsilon)d\epsilon, \quad (10)$$

$$\langle s_z \rangle = -\frac{AU}{2} \int d^3\tilde{S} \exp(-\beta D\tilde{\mathbf{S}}^2)\frac{\langle s_z \rangle - \tilde{S}_z}{\gamma}$$

$$\times \sum_\sigma \sigma \int f(\tilde{\epsilon} + \sigma\gamma)\rho(\epsilon)d\epsilon, \quad (11)$$

where $\gamma = U(\langle s_z \rangle^2 - 2\langle s_z \rangle\tilde{S}_z + \tilde{S}^2)^{1/2}$, $A = (\beta D/\pi)^{3/2}$.

For numerical solution of equations (10) and (11) we keep the value $U = 1.8$ eV which was chosen in Sec. III B for the mean-field analysis and choose temperature-independent $D^{-1} = 0.15$ eV^{-1}, which allows us to achieve the Curie temperature at ambient pressure, which is approximately equal to the experimental value. As in the mean-field approach we solve first the system of equations (10) and (11) for given concentration of electrons $\langle n \rangle$, obtained in DFT, and then compare thermodynamic potentials Ω of para- and ferromagnetic solutions with the same chemical potential (see Appendix B for the explicit expression of Ω for the spin-fermion model).

The obtained dependence of Curie temperature $T_C(p)$ (see Fig. 9) is almost linear and demonstrates a quantitative agreement with the experimental data [5,6]. The position of the first-order quantum phase transition p_c is only weakly changed in comparison to the mean-field theory and therefore remains also close to the experimental value. Therefore, we find that static almost uniform classical spin fluctuations are sufficient to successfully explain the pressure dependence of the Curie temperature, observed experimentally.

Finally, we analyze the temperature dependence of the inverse uniform susceptibility in the mean-field approach and spin-fermion model (see explicit expressions in Appendix B). Our results rescaled with the number of orbitals are shown in the lower panel of Fig. 9 in comparison with the experimental data and the results of DMFT for the single-band model (Fig. 7). We observe that in the region $T > 2000$ K the inverse susceptibility computed by DMFT becomes almost indistinguishable with the mean-field result. This shows correctness
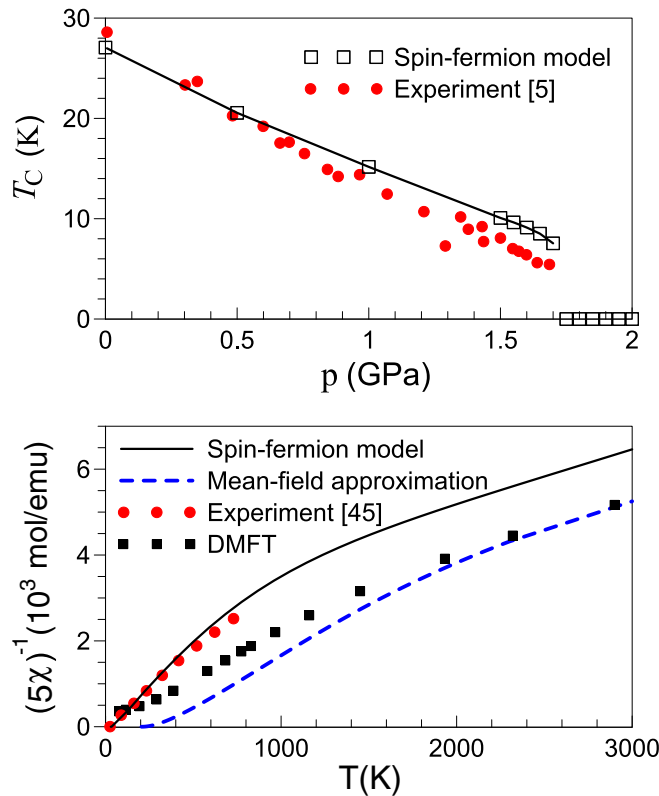
FIG. 9. Magnetic properties of ZrZn$_2$ obtained within spin-fermion model (solid lines) in comparison to the experimental data (circles). Upper panel: Pressure dependence of the Curie temperature $T_C(p)$. The experimental data are taken from Ref. [5]. Lower panel: Temperature dependence of inverse susceptibility, rescaled with the number of orbitals, $[5\chi(T)]^{-1}$ at ambient pressure, compared to the respective results of the mean-field approximation (dashed line), and DMFT for single-band model (squares, cf. Fig. 7). The experimental data are taken from Ref. [45] (without rescaling).

of account of screening of the interaction by choosing a reduced value of the Coulomb interaction in the mean-field approach (cf. Ref. [49]) and confirms a view on the $T > T'_{CW}$ state as on the weakly correlated state. Although at lower temperatures the susceptibility calculated by DMFT is suppressed by local correlations, these correlations, similarly to the results of the multiband model in Fig. 6, are not sufficient to describe the experimental data. At the same time, the result of calculation of uniform magnetic susceptibility within the considered spin-fermion model shows further suppression of susceptibility by nonlocal correlations at moderate temperatures, but at the same time, its enhancement (in comparison to DMFT) in the low-temperature region. The resulting inverse susceptibility closely follows the experimental data. This shows again sufficiency of account of almost uniform classical fluctuations to achieve a good agreement with experiment.

IV. CONCLUSION

In conclusion, by employing a combination of the DFT+DMFT method and analytical model-based techniques we investigated the electronic and magnetic properties of a prototypical itinerant ferromagnet ZrZn$_2$. Our DFT+DMFT

results show that electronic correlations in ZrZn$_2$ are rather weak but not negligible as characterized by an effective mass renormalization of the Zr-4d states $m^*/m \sim 1.1$–1.3. Most importantly, we demonstrate that the 4d t_{2g} electronic states of Zr are partly localized by Coulomb interaction, yielding an orbital-selective formation of local magnetic moments, which are screened at low temperatures.

We also show that the effect of local Coulomb correlations is essential for determining the correct topology of some of the Fermi surface sheets. The shape of the Fermi surface computed by DFT+DMFT supports antiferromagnetic correlations, which compete with the tendency to ferromagnetism and may explain a change of the temperature dependence of resistivity from $T^{5/3}$ to $T^{3/2}$ accompanying the destruction of ferromagnetic order.

Extrapolation of the linear high-temperature part of the inverse uniform susceptibility $\chi^{-1}(T)$ of ZrZn$_2$ calculated by DFT+DMFT to $\chi^{-1}(T) = 0$ yields an estimate of the characteristic temperature of the onset of strong ferromagnetic correlations $T_C^* \sim 32$ K at ambient pressure and $T_C^* \sim 4$ K at $p = 2$ GPa in qualitative agreement with experimental behavior of the Curie temperature.

We would like to emphasize that the peaks of the density of states close to the Fermi level are a rather common feature of many metallic compounds and they can significantly influence the physical properties [51]. In general, these peaks on one hand enhance the tendency to ferromagnetic ordering, but on the other hand, they promote formation of the local moment and the corresponding Kondo screening at low temperatures. The offset of the peak of density of states from the Fermi level increases the corresponding Kondo temperature [35–37,40,46], and, therefore, serves as another source of suppression of ferromagnetism, apart from the suppression of the density of states.

Accordingly, at low temperatures the shape of $\chi^{-1}(T)$, computed by DFT+DMFT, shows a significant deviation from the linear behavior (an upturn). In view of the obtained partial localization of the Zr 4d t_{2g} states this upturn may be explained by a competition of the ferromagnetic ordering with the Kondo effect, which is similar to that considered previously for Kondo lattices [52–57]. This competition was also considered a possible source of weak ferromagnetism [58], and it is expected to be quite sensitive to spatial correlations.

Importance of the Kondo physics for of ZrZn$_2$ is supported by the observation that the shape of $\chi(T)$ obtained by DFT+DMFT is similar to that of FeAl where ferromagnetism is destroyed by the Kondo screening [38]. While the peak of the density of states of ZrZn$_2$ is closer to the Fermi level than that for FeAl, DFT+DMFT for ZrZn$_2$ also yields a paramagnetic ground state, although with a lower temperature of the susceptibility upturn. Since in case of a single impurity the Kondo temperature is typically larger than the Kondo coherence temperature for the lattice, the paramagnetic state in DMFT for ZrZn$_2$ may be a consequence of an overestimate of the Kondo effect by this approach. A possible reason for this overestimate is that suppression of the Kondo effect by nonlocal magnetic correlations is not accounted for by DMFT approach. While the upturn of calculated inverse susceptibility in ZrZn$_2$ can be explained in terms of the Kondo screening, which is overestimated by DMFT, the effect of the approxi-

mations employed within the CT-QMC method, namely Ising-type Hund exchange and the neglect of the effect of spin-orbit coupling, requires further consideration.

We note also that approaching (and even underestimating) the experimental Curie temperature by DFT+DMFT is obtained for such a simple magnet as nickel. Specifically, in this case DMFT approach with Ising [or SU(2)] Hund exchange yields $T_C = 700$ K (or 600 K) [11,59] vs the experimental $T_C = 630$ K. The effective spin of Ni $p = 0.45$ as determined via Eq. (3) using the experimental magnetic moment $\mu = 1.6 \mu_B$ appears to be slightly less than 1/2. This along with the proximity of the Kondo temperature $T_K \approx 800$ K, extracted from the local susceptibility of Ref. [11], to the Curie temperature, also conforms to the presence of a weak Kondo screening in this magnet and shows a possibility of underestimation of the Curie temperature within DFT+DMFT.

To study details of the paramagnet-ferromagnet transition in ZrZn$_2$, we have constructed an effective single-band model by using the Zr 4d contribution to the total density of states. We have shown that for an appropriate choice of the Coulomb repulsion DMFT solution of this model yields results, close to those of the realistic multiband model.

Our results for the effective single-band model obtained within the static mean-field approximation show a second-order paramagnet-ferromagnet phase transition with decreasing temperature at small pressures. Upon increasing pressure the first-order quantum phase transition into the paramagnetic phase occurs in agreement with experimental data. Yet, in contrast to DMFT the static mean-field approximation overestimates the transition temperature by almost an order of magnitude.

To reconcile the results of static and dynamic mean-field approaches to the single-band model, we have also considered a spin-fermion approach to the single-band model. Similarly to DMFT, this approach yields reasonable values of transition temperatures and, at the same time, it preserves the second-order phase transition with changing temperature at low pressures and the first-order quantum phase transition into paramagnetic phase at elevated pressures. Within this model computed pressure dependence of the Curie temperature and the temperature dependence of susceptibility at ambient pressure are in good quantitative agreement with experimental data.

The considered spin-fermion model relies on consideration of ferromagnetic correlations, putting aside other types of correlations and possible Kondo effect (which should be undoubtedly studied in the future). On one hand this approach allows us to obtain physically valuable information about ferromagnetic properties of ZrZn$_2$. Therefore, it is perspective to study magnetic properties of other weak itinerant magnets. On the other hand, this calls for further development of methods describing both local and nonlocal correlations in weak magnets. These approaches can be based on diagrammatic nonlocal extensions of DMFT [60]. Correct treatment of Kondo effect in ZrZn$_2$ may also require account of the nonlocal correlations within the Kondo lattice or periodic Anderson model. Despite these models were intensively applied to describe magnetism of heavy-fermion systems (see, e.g., Ref. [61]), their possible relevance for weak magnets with peaks of the density of states (cf. Ref. [58]) has to be further explored.

APPENDIX A: UNIFORM SUSCEPTIBILITY AT TEMPERATURES HIGHER THE WIDTH OF THE PEAK

We consider the uniform static susceptibility of the multi-band model in the form of a single bubble, Eq. (2) at $\mathbf{q} = 0$,

$$\chi_0 = -2\mu_B^2 T \sum_{\mathbf{k}, i\nu_n, m, m'} G_{\mathbf{k}, mm'}(i\nu_n) G_{\mathbf{k}, m'm}(i\nu_n), \quad \text{(A1)}$$

where $G_{\mathbf{k}, mm'} = \langle c_{k,m,\sigma}^+(0) c_{k,m',\sigma}(\tau) \rangle_{i\nu_n}$ is the electronic Green function, $c_{k,m,\sigma}^+$, $c_{k,m',\sigma}$ are the electron creation and destruction operators with momentum $\mathbf{k}$, orbital m and spin projection σ. Using the spectral representation for the Green's functions we find

$$\chi_0 = -2\mu_B^2 T \sum_{i\nu_n, m, m'} \frac{A_{\mathbf{k}, mm'}(\nu) A_{\mathbf{k}, m'm}(\nu')}{(i\nu_n - \nu)(i\nu_n - \nu')} \quad \text{(A2)}$$

$$= 2\mu_B^2 \sum_{\mathbf{k}, m, m'} \int d\nu \int d\nu' A_{\mathbf{k}, mm'}(\nu) A_{\mathbf{k}, m'm}(\nu')$$

$$\times \frac{f(\nu) - f(\nu')}{\nu' - \nu} \quad \text{(A3)}$$

$$= 2\mu_B^2 \sum_{\mathbf{k}, m, m'} \int d\nu \int d\nu' A_{\mathbf{k}, mm'}(\nu) A_{\mathbf{k}, m'm}(\nu')$$

$$\times [1 - f(\nu)] f(\nu') \frac{\exp[(\nu' - \nu)/T] - 1}{\nu' - \nu}, \quad \text{(A4)}$$

where $A_{\mathbf{k}, mm'}(\nu) = (-1/\pi) \text{Im} G_{\mathbf{k}, mm'}(\nu)$ is the spectral weight of the Green's function, and $f(\nu)$ is the Fermi function. The $1/T$ contribution to susceptibility originates from the integration region $|\nu - \nu'| \ll T$. Together with $\nu \gtrsim -T$ and $\nu' \lesssim T$ restricted by the Fermi functions, this implies $|\nu|, |\nu'| \lesssim T$ in that region.

Let us consider the contribution to the susceptibility from some relevant energy range $\nu, \nu' \in [\epsilon_{\min}, \epsilon_{\max}]$, which contains peaks of the density of states near the Fermi level. In our case this refers to Zr 4d states. The reason is that such contributions, resummed within the random-phase approximation, provide the Curie-Weiss law up to relatively low temperatures $T \gtrsim \max(|\epsilon_{\min}|, \epsilon_{\max})$. Indeed, at $T \gg \max(|\epsilon_{\min}|, \epsilon_{\max})$ we have $|\nu - \nu'| < \epsilon_{\max} - \epsilon_{\min} \ll T$, such that the abovementioned $1/T$ behavior of the bubble takes place. We obtain for

the considered contribution

$$\chi_0 = \frac{2\mu_B^2}{T} \sum_{\mathbf{k},m,m'} \int d\nu \int d\nu' A_{\mathbf{k},mm'}(\nu) A_{\mathbf{k},m'm}(\nu')$$

$$\times [1 - f(\nu)]f(\nu') \tag{A5}$$

$$= \frac{2\mu_B^2}{T} \sum_{\mathbf{k},m,m'} \langle c_{\mathbf{k},m} c_{\mathbf{k},m'}^+ \rangle \langle c_{\mathbf{k},m'}^+ c_{\mathbf{k},m} \rangle. \tag{A6}$$

In the considered temperature range the averages in the last line weakly depend on $\mathbf{k}$ and their local value can be taken, which yields

$$\chi_0 = \frac{4\mu_B^2}{3T} \langle S^2 \rangle = \frac{\mu^2}{3T}, \tag{A7}$$

where $\langle S^2 \rangle$ is the average square of spin on the relevant orbitals ($4d$ Zr in our case). For ZrZn$_2$ we obtain from DFT+DMFT calculations of the multiorbital model $\langle S^2 \rangle =$ 1.43. This yields a corresponding magnetic moment $\mu =$ 2.39 μ_B, which agrees well with the moment extracted from inverse susceptibility in the temperature range $T > T'_{\mathrm{CW}}$ (see Sec. II B 4). Note that obtained in DFT+DMFT intraorbital contributions to this value, $\mu = ((3/2) \sum_m n_m(2 - n_m))^{1/2} \mu_B = 2.16 \mu_B$, so that the interorbital correlations are relatively weak.

The results (A6) and (A7) can be extended to the uniform susceptibility in DMFT, which can be represented in the form [24,60]

$$\chi_{\mathbf{q}=0}^{\mathrm{DMFT}} = 2\mu_B^2 \sum_{\substack{\nu, m, m', \\ \nu', m'', m'''}} \left[\delta_{\nu\nu'} \hat{\chi}_{0,\nu}^{-1} - \hat{\Gamma} \right]_{\substack{\nu m m', \\ \nu' m'' m'''}}^{-1}, \tag{A8}$$

where $\hat{\chi}_0$ is the matrix in orbital indexes of the bubbles of Green's functions, similar to the Eq. (A1),

$$\hat{\chi}_{0,\nu}^{mm',m''m'''} = -T \sum_{\mathbf{k}} G_{\mathbf{k},mm''}(i\nu) G_{\mathbf{k},m'''m'}(i\nu),$$

and $\hat{\Gamma}$ is the irreducible vertex (which is also considered as a matrix in frequency and orbital space). Assuming that the vertex Γ is weakly frequency and orbital dependent, using spectral representation for Green's functions, which is similar to that in Eq. (A4) and considering the contribution of the energy range $|\nu|, |\nu'| \lesssim T$, we arrive at the random-phase approximation (RPA)-like results for the susceptibility, which fulfills the Curie-Weiss law, with the Curie constant given approximately by Eq. (A7). The main effect of the vertex Γ in this case is in the shift of the inverse susceptibility with respect to the Curie law (A7), i.e., introducing a finite Weiss temperature.

APPENDIX B: DERIVATION OF THE EQUATIONS OF THE SPIN-FERMION MODEL

The action (9) can be written as the quadratic form of fermionic operators as follows:

$$\mathcal{S}_{\mathrm{eff}} = \sum_{k,\sigma,\sigma'} c_{k,\sigma}^\dagger M_{\sigma,\sigma'}(k) c_{k,\sigma'} + D\tilde{\mathbf{S}}^2 + E_0, \tag{B1}$$

where $E_0 = U(\langle s_z \rangle^2 - \langle n \rangle^2/4)$,

$$\mathbf{M} = \begin{pmatrix} -i\nu_n + \tilde{\epsilon}_{\mathbf{k}} - H_{\mathrm{MF}}/2 + U\tilde{S}_z & U(\tilde{S}_x - i\tilde{S}_y) \\ U(\tilde{S}_x + i\tilde{S}_y) & -i\nu_n + \tilde{\epsilon}_{\mathbf{k}} + H_{\mathrm{MF}}/2 - U\tilde{S}_z \end{pmatrix}, \tag{B2}$$

$H_{\mathrm{MF}} = H + 2U \langle s_z \rangle$, we have added the magnetic field H for completeness, and

$$\tilde{\epsilon}_{\mathbf{k}} = \epsilon_{\mathbf{k}} - \mu + \frac{U \langle n \rangle}{2}.$$

After integrating out the fermions in Eq. (8), we get the partition function Z in the form

$$Z = e^{-\beta E_0} \int d^3\tilde{S} \exp\left(-\beta D\tilde{\mathbf{S}}^2 + \sum_{\mathbf{k},n} \ln(\beta^2 \det \mathbf{M}) \right). \tag{B3}$$

Using Eq. (B2), we obtain

$$\det \mathbf{M} = (-i\nu_n + \tilde{\epsilon}_{\mathbf{k}})^2 - \gamma^2, \tag{B4}$$

where

$$\gamma^2 = H_{\mathrm{MF}}^2/4 - UH_{\mathrm{MF}}\tilde{S}_z + U^2\tilde{S}^2. \tag{B5}$$

The Matsubara sum in Eq. (B3) can be carried out exactly, yielding

$$\sum_{\mathbf{k},n} \ln(\beta^2 \det \mathbf{M}) = \sum_{\mathbf{k},n,\sigma} \ln(\beta(-i\nu_n + \tilde{\epsilon}_{\mathbf{k}} + \sigma\gamma))$$

$$= -\sum_{\mathbf{k},\sigma} \ln(1 - f(\tilde{\epsilon}_{\mathbf{k}} + \sigma\gamma)). \tag{B6}$$

Substituting this result in Eq. (B3), the partition function finally becomes

$$Z = e^{-\beta E_0} \int d^3\tilde{S} \exp(-\beta D\tilde{\mathbf{S}}^2 - R(\tilde{\mathbf{S}})), \tag{B7}$$

where $R(\tilde{\mathbf{S}}) = \sum_\sigma \int d\epsilon \rho(\epsilon) \ln(1 - f(\tilde{\epsilon} + \sigma\gamma))$. Therefore, in the presented spin-fermion model, the average total occupation $\langle n \rangle$ is given by

$$\langle n \rangle = -\frac{\partial \Omega}{\partial \mu} = \frac{e^{-\beta E_0}}{Z} \int d^3\tilde{S} \exp(-\beta D\tilde{\mathbf{S}}^2 - R(\tilde{\mathbf{S}}))$$

$$\times \left[\sum_\sigma \int f(\tilde{\epsilon} + \sigma\gamma)\rho(\epsilon) d\epsilon \right] \tag{B8}$$

and the average magnetization $\langle s_z \rangle$ is

$$\langle s_z \rangle = -\frac{\partial \Omega}{\partial H} = -\frac{e^{-\beta E_0}}{Z} \int d^3\tilde{S} \exp(-\beta D\tilde{\mathbf{S}}^2 - R(\tilde{\mathbf{S}}))$$

$$\times \left[\sum_\sigma \sigma \int \frac{\frac{H_{\mathrm{MF}}}{2} - U\tilde{S}_z}{2\gamma} f(\tilde{\epsilon} + \sigma\gamma)\rho(\epsilon) d\epsilon \right], \tag{B9}$$

where $\Omega = -\beta^{-1} \ln Z$ is the thermodynamic potential.

The expansion of logarithmic contribution $R(\tilde{\mathbf{S}})$ in the exponents of Eqs. (B7)–(B9) in powers of γ contains only even powers and corresponds to weak magnetization of the spin-fluctuation field (the first order in $\tilde{S}$ term), the renormalization of the value of D (for the second-order term), and multiparamagnon interactions (higher-order terms). We neglect the weak magnetic field acting on $\tilde{S}$ and multiparamagnon

interactions effects and assume that the value of D is already renormalized. These approximations imply replacement of γ in these logarithmic contributions by its $\tilde{S} = 0$ value. At fixed $\langle n \rangle = 2 \int_{-\infty}^{\epsilon_F} \rho(\epsilon) d\epsilon$, $H = 0$, T, D, the equations (B8) and (B9) reduce therefore to the equations (10) and (11) of the main text.

To calculate the susceptibility we differentiate Eq. (B9), neglecting the logarithmic contribution in the exponent, over H. Using

$$\frac{dH_{MF}}{dH} = 1 + 2U\chi_s, \tag{B10}$$

where $\chi_s = d\langle s_z \rangle / dH$, we find at $H \to 0$

$$\frac{d\gamma}{dH} = \frac{U}{2\gamma}(\langle s_z \rangle - \tilde{S}_z)(1 + 2U\chi_s),$$

$$\frac{d}{dH}\left(\frac{H_{MF}/2 - U\tilde{S}_z}{2\gamma}\right) = U^2 \frac{\tilde{S}_x^2 + \tilde{S}_y^2}{4\gamma^3}(1 + 2U\chi_s). \tag{B11}$$

In the following we assume paramagnetic phase $\langle s_z \rangle = 0$. In this case the derivative $d\mu/dH$ does not contribute to the susceptibility χ since the corresponding term is odd in $\tilde{S}_z$. Collecting all the terms together we obtain RPA-like result

$$\chi = 4\mu_B^2 \chi_s = 2\mu_B^2 \frac{\chi_0^{SF}}{1 - U\chi_0^{SF}}, \tag{B12}$$

where

$$\chi_0^{SF} = (2Z_0)^{-1} \sum_\sigma (F^\sigma - \sigma D^\sigma), \tag{B13}$$

we have introduced

$$F^\sigma = \frac{4\pi}{3} \int_0^\infty d\tilde{S} \tilde{S}^2 B^\sigma(\tilde{S}) \exp(-\beta D\tilde{\mathbf{S}}^2), \tag{B14}$$

$$D^\sigma = \frac{8\pi}{3U} \int_0^\infty d\tilde{S} \tilde{S} A^\sigma(\tilde{S}) \exp(-\beta D\tilde{\mathbf{S}}^2), \tag{B15}$$

and

$$A^\sigma(\tilde{S}) = \int f(\tilde{\epsilon} + \sigma\gamma)\rho(\epsilon)d\epsilon, \tag{B16}$$

$$B^\sigma(\tilde{S}) = -\int \frac{\partial f(\tilde{\epsilon} + \sigma\gamma)}{\partial \epsilon}\rho(\epsilon)d\epsilon, \tag{B17}$$

$$Z_0 = \int d^3\tilde{S} \exp(-\beta D\tilde{\mathbf{S}}^2). \tag{B18}$$

Integrating by parts, equation (B15) can be written as

$$D^\sigma = \frac{4\pi}{3\beta DU}\left[A^\sigma(0) - \sigma U \int_0^\infty d\tilde{S} B^\sigma(\tilde{S}) \exp(-\beta D\tilde{\mathbf{S}}^2)\right]. \tag{B19}$$

Substituting Eqs. (B19) into Eq. (B13), we obtain

$$\chi_0^{SF} = \frac{2\pi}{3Z_0}\int_0^\infty d\tilde{S}\left(\tilde{S}^2 + \frac{1}{\beta D}\right)\sum_\sigma B^\sigma(\tilde{S}) \exp(-\beta D\tilde{\mathbf{S}}^2). \tag{B20}$$

In the absence of spin fluctuations ($D \to \infty$), i.e., in mean-field approach, we find the RPA result of Eq. (B12) with $\chi_0^{SF} \to -\int \rho(\epsilon)f'(\tilde{\epsilon})d\epsilon$, which is the bare spin susceptibility. The resulting temperature dependence of the inverse susceptibility in the mean-field and spin-fermion model is discussed in Sec. III C.

[1] B. T. Matthias and R. M. Bozorth, Phys. Rev. **109**, 604 (1958).

[2] T. F. Smith, J. A. Mydosh, and E. P. Wohlfarth, Phys. Rev. Lett. **27**, 1732 (1971).

[3] C. Pfleiderer, M. Uhlarz, S. M. Hayden, R. Vollmer, H. V. Lohneysen, N. R. Bernhoeft, and G. G. Lonzarich, Nature (London) **412**, 58 (2001).

[4] R. P. Smith, M. Sutherland, G. G. Lonzarich, S. S. Saxena, N. Kimura, S. Takashima, M. Nohara, and H. Takagi, Nature (London) **455**, 1220 (2008).

[5] M. Uhlarz, C. Pfleiderer, and S. M. Hayden, Phys. Rev. Lett. **93**, 256404 (2004).

[6] N. Kabeya, H. Maekawa, K. Deguchi, N. Kimura, H. Aoki1, and N. K. Sato, Phys. Status Solidi B **250**, 654 (2013).

[7] S. Ogawa, J. Phys. Soc. Jpn. **40**, 1007 (1976).

[8] T. Moriya, *Spin fluctuations in Itinerant Electron Magnetism* (Springer, Berlin, Heidelberg, 1985).

[9] D. Linton Johnson, Phys. Rev. B **9**, 2273 (1974).

[10] M.-C. Huang, H. J. F. Jansen, and A. J. Freeman, Phys. Rev. B **37**, 3489 (1988).

[11] A. Hausoel, M. Karolak, E. Şaşıoğlu, A. Lichtenstein, K. Held, A. Katanin, A. Toschi, and G. Sangiovanni, Nat. Commun. **8**, 16062 (2017).

[12] E. Bruno, B. Ginatempo, and J. B. Staunton, Phys. Rev. B **65**, 092503 (2002).

[13] E. P. Wohlfarth, J. Appl. Phys. **39**, 1061 (1968).

[14] V. Yu. Irkhin, A. A. Katanin, and M. I. Katsnelson, Phys. Rev. B **64**, 165107 (2001); C. Honerkamp and M. Salmhofer, *ibid.* **64**, 184516 (2001).

[15] A. J. Millis, Phys. Rev. B **48**, 7183 (1993).

[16] J. A. Hertz and M. A. Klenin, Phys. Rev. B **10**, 1084 (1974).

[17] A. A. Katanin, Phys. Rev. B **72**, 035111 (2005).

[18] P. A. Igoshev, A. A. Katanin, and V. Yu. Irkhin, J. Exp. Theor. Phys. **105**, 1043 (2007).

[19] P. A. Igoshev, A. A. Katanin, H. Yamase, and V. Yu. Irkhin, J. Magn. Magn. Mater. **321**, 899 (2009).

[20] P. Werner, E. Gull, M. Troyer, and A. J. Millis, Phys. Rev. Lett. **101**, 166405 (2008).

[21] Z. P. Yin, K. Haule, and G. Kotliar, Nat. Mater. **10**, 932 (2011).

[22] A. S. Belozerov, A. A. Katanin, and V. I. Anisimov, Phys. Rev. B **97**, 115141 (2018).

[23] W. Metzner and D. Vollhardt, Phys. Rev. Lett. **62**, 324 (1989).

[24] A. Georges, G. Kotliar, W. Krauth, and M. J. Rozenberg, Rev. Mod. Phys. **68**, 13 (1996).

[25] V. I. Anisimov, A. I. Poteryaev, M. A. Korotin, A. O. Anokhin, and G. Kotliar, J. Phys. Condens. Matter **9**, 7359 (1997); A. I. Lichtenstein and M. I. Katsnelson, Phys. Rev. B **57**, 6884 (1998).

[26] G. Kotliar, S. Y. Savrasov, K. Haule, V. S. Oudovenko, O. Parcollet, and C. A. Marianetti, Rev. Mod. Phys. **78**, 865 (2006); J. Kuneš, I. Leonov, P. Augustinský, V. Křápek, M. Kollar, and D. Vollhardt, Eur. Phys. J. Spec. Top. **226**, 2641 (2017).

[27] S. Baroni, S. de Gironcoli, A. Dal Corso, and P. Giannozzi, Rev. Mod. Phys. **73**, 515 (2001); P. Giannozzi, S. Baroni, N. Bonini, M. Calandra, R. Car *et al.*, J. Phys.: Condens. Matter **21**, 395502 (2009).

[28] N. Marzari, A. A. Mostofi, J. R. Yates, I. Souza, and D. Vanderbilt, Rev. Mod. Phys. **84**, 1419 (2012).

[29] V. I. Anisimov, D. E. Kondakov, A. V. Kozhevnikov, I. A. Nekrasov, Z. V. Pchelkina, J. W. Allen, S.-K. Mo, H.-D. Kim, P. Metcalf, S. Suga, A. Sekiyama, G. Keller, I. Leonov, X. Ren, and D. Vollhardt, Phys. Rev. B **71**, 125119 (2005); Dm. Korotin, A. V. Kozhevnikov, S. L. Skornyakov, I. Leonov, N. Binggeli, V. I. Anisimov, and G. Trimarchi, Eur. Phys. J. B **65**, 91 (2008).

[30] P. Werner, A. Comanac, L. de Medici, M. Troyer, and A. J. Millis, Phys. Rev. Lett. **97**, 076405 (2006); E. Gull, A. J. Millis, A. I. Lichtenstein, A. N. Rubtsov, M. Troyer, and P. Werner, Rev. Mod. Phys. **83**, 349 (2011).

[31] E. Şaşıoğlu, C. Friedrich, and S. Blügel, Phys. Rev. B **83**, 121101(R) (2011); Y. Si, H.-Y. Wu, H.-M. Yang, W.-Q. Huang, K. Yang, P. Peng, and G.-F. Huang, Nanoscale Res. Lett. **11**, 495 (2016)

[32] H. J. Vidberg and J. W. Serene, J. Low Temp. Phys. **29**, 179 (1977).

[33] F. Birch, Phys. Rev. **71**, 809 (1947).

[34] J. Kübler, Phys. Rev. B **70**, 064427 (2004).

[35] A. A. Katanin, A. I. Poteryaev, A. V. Efremov, A. O. Shorikov, S. L. Skornyakov, M. A. Korotin, and V. I. Anisimov, Phys. Rev. B **81**, 045117 (2010).

[36] P. A. Igoshev, A. V. Efremov, A. I. Poteryaev, A. A. Katanin, and V. I. Anisimov, Phys. Rev. B **88**, 155120 (2013).

[37] A. S. Belozerov, A. A. Katanin, V. Yu. Irkhin, and V. I. Anisimov, Phys. Rev. B **101**, 155126 (2020).

[38] A. Galler, C. Taranto, M. Wallerberger, M. Kaltak, G. Kresse, G. Sangiovanni, A. Toschi, and K. Held, Phys. Rev. B **92**, 205132 (2015).

[39] A. Liebsch and A. Lichtenstein, Phys. Rev. Lett. **84**, 1591 (2000).

[40] S. L. Skornyakov, V. I. Anisimov, and D. Vollhardt, Phys. Rev. B **86**, 125124 (2012).

[41] S. L. Skornyakov, V. I. Anisimov, D. Vollhardt, and I. Leonov, Phys. Rev. B **96**, 035137 (2017).

[42] Zs. Major, S. B. Dugdale, R. J. Watts, G. Santi, M. A. Alam, S. M. Hayden, J. A. Duffy, J. W. Taylor, T. Jarlborg, E. Bruno, D. Benea, and H. Ebert, Phys. Rev. Lett. **92**, 107003 (2004).

[43] H. R. Krishna-murthy, J. W. Wilkins, and K. G. Wilson, Phys. Rev. B **21**, 1003 (1980).

[44] A. Toschi, R. Arita, P. Hansmann, G. Sangiovanni, and K. Held, Phys. Rev. B **86**, 064411 (2012).

[45] M. Shimizu and H. Okada, Phys. Lett. A **85**, 474 (1981).

[46] S. L. Skornyakov, A. A. Katanin, and V. I. Anisimov, Phys. Rev. Lett. **106**, 047007 (2011).

[47] J. Wahle, N. Blümer, J. Schlipf, K. Held, and D. Vollhardt, Phys. Rev. B **58**, 12749 (1998).

[48] T. Kanamori, Prog. Theor. Phys. **30**, 275 (1963).

[49] A. A. Katanin, H. Yamase, and V. Yu. Irkhin, J. Phys. Soc. Jpn. **80**, 063702 (2011).

[50] J. Schmalian, D. Pines, and B. Stojkovic, Phys. Rev. Lett. **80**, 3839 (1998); Phys. Rev. B **60**, 667 (1999).

[51] S. V. Vonsovskii, M. I. Katsnelson, and A. V. Trefilov, Phys. Met. Metallogr. **76**, 247 (1993).

[52] Z. Li, M. Zhuang, and M. Xiao, J. Phys.: Condens. Matter **8**, 7941 (1996).

[53] F. J. Ohkawa, Phys. Rev. B **65**, 174424 (2002).

[54] S. J. Yamamoto and Q. Si, PNAS **107**, 15704 (2010).

[55] G.-B. Li, G.-M. Zhang, and Lu Yu, Phys. Rev. B **81**, 094420 (2010); Y. Liu, G.-M. Zhang, and L. Yu, *ibid.* **87**, 134409 (2013).

[56] S. Hoshino and Y. Kuramoto, Phys. Rev. Lett. **111**, 026401 (2013).

[57] K. Kubo, Phys. Rev. B **87**, 195127 (2013); J. Phys. Soc. Jpn. **84**, 094702 (2015).

[58] V. Yu. Irkhin, J. Phys.: Condens. Matter **23**, 065602 (2011); J. Exp. Theor. Phys. **125**, 159 (2017).

[59] A. I. Lichtenstein, M. I. Katsnelson, and G. Kotliar, Phys. Rev. Lett. **87**, 067205 (2001).

[60] G. Rohringer, H. Hafermann, A. Toschi, A. A. Katanin, A. E. Antipov, M. I. Katsnelson, A. I. Lichtenstein, A. N. Rubtsov, and K. Held, Rev. Mod. Phys. **90**, 025003 (2018).

[61] Hewson, *A. C. The Kondo Problem to Heavy Fermions* (Cambridge Univ. Press, Cambridge, 1993); M. Lavagna and C. Pépin, Acta Phys. Pol. B **29**, 3753 (1998); B. Coqblin, M. D. Núñez-Regueiro, A. Theumann, J. R. Iglesias, and S. G Magalhães, Phil. Mag. **86**, 2567 (2006); C. D. Batista, J. Bonca, and J. E. Gubernatis, Phys. Rev. B **68**, 214430 (2003)